Design and fabrication of a silica optical micro-kayak cavity on a silicon chip

Yantang Huang (黄衍堂)*, Changlei Guo (郭长磊), Riyan Bao (鲍日焰), and Xiaohua Wang (王晓花)

College of Physics and Information Engineering, Fuzhou University, Fuzhou 350108, China

**Corresponding author: huangyantang@fzu.edu.cn*

Received November 15, 2012; accepted January 25, 2013; posted online April 10, 2013

A new type of silica optical micro-kayak cavity fabricated on a silicon chip is designed and demonstrated. This micro-kayak cavity with two straight sides and two semi-circle sides can be used to achieve a compact and flexible arrangement in the design of integrated photonic circuits. The micro-kayak cavity can also be embedded with a Bragg reflection grating in the straight sides for frequency selection using a micro-kayak cavity laser doped with a rare-earth ion. We describe the fabrication methods for the micro-kayak cavity, obtain its spectra, and discuss its potential applications.

OCIS codes: 220.4000, 140.4780.

doi: 10.3788/COL201311.052201.

Optical microcavity resonators have distinct features because of their whispering-gallery modes (WGMs) compared with Fabry–Perot resonators, which have confined modes. In a microcavity resonator, the light is continuously bounced back from a dielectric curved cavity boundary by total internal reflection. Moreover, optical microcavity resonators can spatially and temporally compress coupling light. Thus, these resonators are attracting considerable attention[1] in fundamental studies on cavity quantum electrodynamics[2−4] and nonlinear optical effects[5−6], as well as in devices such as low-threshold microscale lasers[7−8], passive photonic devices[9], and biochemical sensors[10−11].

Optical microcavities[1] can be in the form of microspheres[7], microdisks[12], or microtoroids[4,8]. In this letter, we design and demonstrate a surface-tension-induced optical microcavity with a new structure, i.e., a kayak-like shape, and called it an optical micro-kayak cavity. The photomicrograph of the silica optical micro-kayak cavity on a silicon chip is shown in Fig. 1.

The same as a microtoroid cavity[13], the surface-tension-induced micro-kayak cavity has significantly low number of excited WGMs and a high quality (Q) factor, i.e., a low intrinsic loss. This property can be attributed to the near-atomic smoothness of the surface quality and low material loss window of silica.

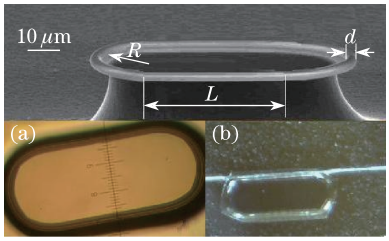

Fig. 1. Silica optical microcavity with a kayak-like shape on a silicon chip. The main figure shows the scanning electron micrograph of the micro-kayak cavity with semi-circle radius R, straight-side length L, and minor diameter d. Inset (a) is the photomicrograph of the micro-kayak cavity; inset (b) is the photomicrograph of the micro-kayak cavity coupled with optical tapered fiber.

However, the microtoroid cavity has not the two straight sides. Due to the free spectral range ($\Delta\nu_{\mathrm{FSR}}$) and the morphology characteristics spectra which are related with the refractive index and circumference[13], this kind of microcavity has extra straight sides length to adjust the free spectral range and the center wavelength of resonance. We can construct filters for optical fiber communication networks based on the standard center wavelength, such as optical comb filters. In addition, the two straight sides increase the micro-kayak cavity circumference. We can design the optical micro-kayak cavity with a small semi-circle diameter D, which confers plasticity for integrated light path arrangement and compactness. The straight side of micro-kayak cavity lasers doped with rare-earth ions can be embedded with a Bragg reflection grating similar to an optical fiber grating for frequency selection. Here, we demonstrate a method of producing silica micro-kayak cavity resonators on a chip using a combination of lithography, wet etching, and selective reflow process[13]. The characteristic spectra of the optical micro-kayak cavities were then obtained.

Racetrack silica disks were fabricated on a silicon substrate using the same process as that previously described for fabricating silica disk microcavities on a silicon substrate[13]. The fabrication process flow involved several steps. Silicon wafers were first prepared using a 1.2 to 2.0-μm layer of silicon dioxide (SiO_2) grown by wet thermal oxidation in a horizontal tube furnace. Photolithography was performed to create disk-shaped photoresist pads on a primary-grade silicon (100) substrate. The pattern was then transferred onto the SiO_2 layer. Afterwards, selective dry or wet etching of the exposed silicon was conducted. To separate the racetrack disk suspension from the silicon, the silicon under the silica disk was etched. The silicon pillars supporting the racetrack SiO_2 disks were maintained. Silicon etching includes two methods, namely, dry etching and wet etching. Dry etching uses gases such as XeF_2[14] and FS_6[15], but these gases are toxic and the equipment is expensive. In this letter, isotropic and anisotropic wet etching were conducted to remove silicon selectively.

In the anisotropic wet etching process, the racetrack disk of the photoresist served as an etch mask during immersion in buffered hydrofluoric acid (HF) solution at room temperature. Acetone was used to remove residual photoresist and organic contamination. The remaining SiO_2 disks served as protection masks during immersion in the anisotropic selective removal of silicon solution. Tetramethylammonium hydroxide (TMAH) solution (25 wt.-%) was used for the anisotropic selective removal of silicon. The TMAH solution container was warmed at 80 °C in a water bath, and a p-type silicon (100) wafer was used. Given that silicon is an anisotropic crystal, the shape of the remaining silicon pillar is related to the orientation of the photolithography mask. Thus, after a certain period of etching, the racetrack SiO_2 disk stood atop a silicon pillar with sharp corners, as shown in Fig. 2.

We also adopted silicon isotropic etching using a HNO_3:HF (5:1) solution. The etching rate was almost equal in all directions. Given that the isotropic wet etching solution contained HF, a part of the silica film was corroded during silicon etching. The etching model is shown in Fig. 3.

Silicon etching was conducted along the vertical and horizontal directions so that the ultimate edge of the silica disk was wedge shaped. An appropriate etching duration was required to achieve the largest possible width of silica outside the silicon pillar. The large width of silica benefited the fabrication of the micro-kayak cavity with an appropriately small diameter. The sample was immersed in etching solution for 120 s. Then, the sample was removed from the solution and cleaned with deionized water. The transverse depth of the silicon etching in the center is approximately 15 μm. The width of the silica outside the silicon pillar is approximately 10 μm, as shown in Fig. 4. The cross-section of the remaining

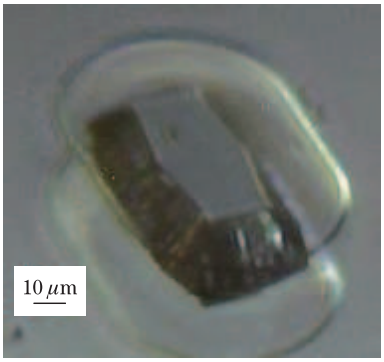

Fig. 2. Photomicrograph of the micro-racetrack silica disk after anisotropic etching.

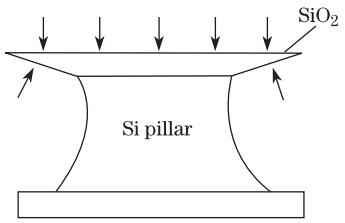

Fig. 3. Model of silicon isotropic wet etching.

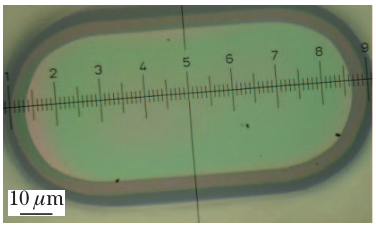

Fig. 4. Photomicrograph of the racetrack disk after isotropic wet etching for 120 s.

silicon pillar has no sharp corners, which is the same as the silica mask, because of silicon isotropic etching. This shape is in favour of the high quality factor (Q) of the micro-kayak resonator. However, the silicon pillar is relatively short.

To exploit the advantages of the two methods, anisotropic silicon wet etching was first conducted for 10 s, followed by isotropic wet etching process for several seconds more.

The periphery of the racetrack silica disk suspension is rough, resulting in a low Q factor of the microcavity. A processing step using a CO_2 laser (10.6-μm wavelength) was conducted to selectively heat and allow the reflow of the SiO_2 racetrack disk suspension without affecting the silicon support pillar[13]. The melting points of silica and silicon are 1 710 °C and 1 420 °C, respectively. However, silicon has a far weaker optical absorption and is 100 times more thermally conductive than silica at 10.6 μm[16,17]. Therefore, the silicon pillar remains significantly cooler and physically unaffected throughout the silica reflow process, ensuring that most of the energy is absorbed by the silica than the silicon. The silicon supporting pillar does not melt or deform. Figure 5 shows the melting device. The CO_2 laser used has a maximum optical power of 80 W and was controlled using a software program to adjust the power and sustain time of the output laser. Laser light (10.6 μm) was reflected and focused on the stage. The silicon chip with a racetrack disk was laid on a metal rotatable stage, which was installed on a three-dimensional adjustment frame. A microscopic charge-coupled device (CCD) with a magnification of 400× was used to observe the process.

The certain area of the racetrack SiO_2 disk edge was initially surface-normal irradiated by a CO_2 laser with 5 – 12 W power for a few minutes, and then this area was melted. The rim rolled up because of the induced surface tension. A smooth annular surface formed and continued until self-stopping. The stage was slowly rotated, and the three-dimensional (3D) frame was adjusted to conduct a melting scan of each zone of the whole microdisk. The presence of insufficiently melted areas was determined using a microscope. If insufficiently melted parts were observed, this part would be irradiated with 1 to 2 W increments of laser power.

A tension-induced, nanoscale smooth optical micro-kayak cavity is produced. Figure 5(b) shows the micro-kayak cavity with a straight side L of 75 μm, semi-circle radius R of 50 μm, and minor diameter d of approximately 2.5 μm.

The optical tapered fiber is the best coupler for light field coupling into microcavity WGMs[8]. In this letter a optical tapered fiber was used to obtain the characteristic morphological spectra of the micro-kayak res-

onator, which allowed coupling in the straight or semicircular side. The tapered fiber was formed by stretching a standard optical fiber while heating it with a hydrogen flame[7,8] or etching a standard optical fiber with HF solution[18]. The resulting tapered fiber exhibits a tapered waist diameter from 1.5 to 2.5 μm, and the losses are typically less than 5%. These parameters were adjusted to phase match the resonator appropriately. We designed an adjustable platform for the coupling of the optical fiber and micro-kayak cavity, as shown in Fig. 6. A U-shaped frame with a tapered fiber was fixed on the three-dimensional adjustment platform. Proper alignment was ensured so that the optical tapered fiber was parallel and tangent to the straight side (or semicircular side) of the micro-kayak cavity. Two optical microscopes with a CCD (~400× magnification) were used to photograph the micro-kayak resonators and tapered fiber simultaneously from the top and side.

An amplified spontaneous emission broadband light source with a C+L band (1 520 to 1 610 nm) as working wavelength was used to measure the transmission spectra of the tapered fiber coupled with the micro-kayak resonator. One end of the tapered fiber was connected to the light source. The output power ranged from 2 to 20 mW. Better spectral flat characteristics were achieved within the working bandwidth. The other end was connected to an AQ6370 optical spectrum analyzer (OSA).

Figure 7 shows the characteristic normalized optical transmission spectra with high Q of the 464-μm-circumference micro-kayak cavity (Fig. 5(b)). The filter depth (extinction ratio) of the micro-kayak cavity is approximately 13 dB, and the spectrum linewidth is 0.25 nm at 1 550.40 nm. The Q value is 6.2×10^3, which is relatively low because of the following reasons: a) the straight side mode is mismatched with the circular mode; b) the minimum resolution of the OSA is only 0.02 nm; c) the micro-kayak cavity sample may be contaminated, thereby sharply reducing the Q value. The measured non-resonant insertion loss during the experiment is less than 0.5 dB. The observed free spectral range corresponding to the equatorial mode number (l-index) is 3.3 nm. The free spectral range of the micro-kayak cavity is calculated as[19]

$$\Delta\lambda_{\mathrm{FSR}} \approx \frac{\lambda^2}{n_{\mathrm{eff}}(2L+2\pi R)}, \quad (1)$$

where n_{eff} and $2L+2\pi$R are the effective refractive index and circumference of the micro-kayak cavity, respectively. The effective index of silica grown by thermal oxidation at 1 550-nm wavelength is approximately 1.45. The circumference is 464 μm based on optical microscopy measurements, and the calculated free spectral range is 3.5 nm. This relatively large mode spacing is one of the reasons that microresonators are gaining significant interest in the fields of telecommunications (as channel-dropping components)[9], single-mode laser sources[8], etc. We fabricated several micro-kayak cavities to show the good reproducibility of the optical properties. We found that this photonic device may be used in 50-GHz comb filters for optical fiber communication networks.

In conclusion, we demonstrate a process for producing

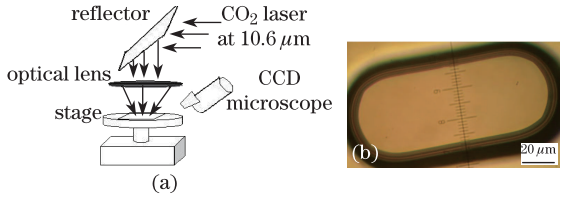

Fig. 5. (a) Setup of the 10.6-μm CO_2 laser for melting the racetrack SiO_2 disk. (b) Photomicrograph of the micro-kayak cavity on a racetrack disk after CO_2 laser melting.

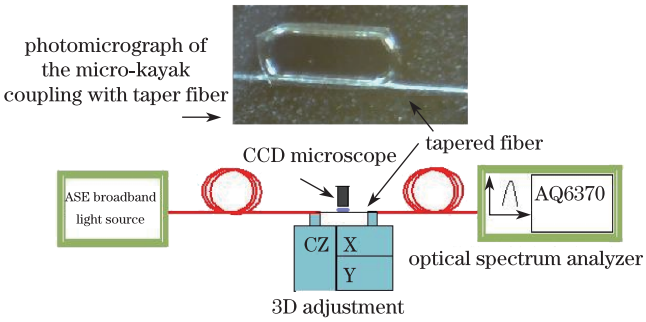

Fig. 6. Schematic of the measurement device. The inset is the photomicrograph of a tapered fiber tangent to the micro-kayak cavity.

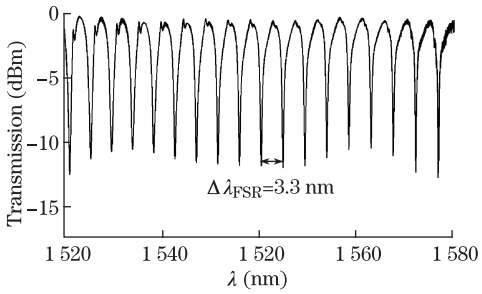

Fig. 7. Normalized optical transmission spectra of a micro-kayak cavity with a 464-μm circumference.

kayak-shaped silica microresonators on a chip using a combination of lithography, wet etching, and selective reflow process. We experimentally measure the characteristic morphological spectra and filtering performance of the micro-kayak cavity, free spectral range, and full-width at half-maximum linewidth. The experimental results show that the micro-kayak cavity has a free spectral range of 3.3 nm and extinction ratio of approximately 13 dB. We believe that the micro-kayak resonator can be used in many optical signal processing devices such as photonic devices in dense wavelength-division multiplexing optical fiber communication networks. The micro-kayak cavity also has potential applications in comb filters, wavelength-division multiplexers, add and drop multiplexer, as well as single-frequency microcavity lasers on a chip.

This work was supported by the Natural Science Foundation of Fujian Province of China under Grant No. A0610016.

References

1. K. J. Vahala, Nature **424,** 839 (2003).

2. D. Vernooy, A. Furusawa, N. Georgiades, V. Ilchenko, and H. Kimble, Phys. Rev. A **57,** R2293 (1998).
3. S. Spillane, T. Kippenberg, K. Vahala, K. Goh, E. Wilcut, and H. Kimble, Phys. Rev. A **71,** 013817 (2005).
4. R. Bao, X. Wang, and Y. Huang, Chin. Phys. Lett. **27,** 083101 (2010).
5. S. M. Spillane, T. J. Kippenberg, and K. J. Vahala, Nature **415,** 621 (2002).
6. T. J. Kippenberg, S. M. Spillane, and K. J. Vahala, Phys. Rev. Lett. **93,** 083904 (2004).
7. M. Cai and K. Vahala, Opt. Lett. **26,** 884 (2001).
8. L. Yang, D. Armani, and K. Vahala, Appl. Phys. Lett. **83,** 825 (2003).
9. H. Rokhsari and K. Vahala, Phys. Rev. Lett. **92,** 253905 (2004).
10. S. Arnold, M. Khoshsima, I. Teraoka, S. Holler, and F. Vollmer, Opt. Lett. **28,** 272 (2003).
11. A. T. Rosenberger, Opt. Express **15,** 12959 (2007).
12. H. Lee, T. Chen, J. Li, K. Y. Yang, S. Jeon, O. Painter, and K. J. Vahala, Nature Photon. **6,** 369 (2012).
13. D. K. Armani, T. J. Kippenberg, S. M. Spillane, and K. J. Vahala, Nature **421,** 925 (2003).
14. U. Streller, A. Krabbe, and N. Schwentner, Appl. Surf. Sci. **106,** 341 (1996).
15. E. Gogolides, C. Boukouras, G. Kokkorisetal, O. Brani, A. Tserepi, and V. Constantoudis, Micro. Electron. Eng. **73,** 312 (2002).
16. A. D. McLachlan and F. P. Meyer, Appl. Opt. **26,** 1728 (1987).
17. M. Sheik-bahae and H. S. Kwok, J. Appl. Phys. **63,** 518 (1988).
18. Y. Huang, X. Wang, and R. Bao, Appl. Mechan. Mater. **145,** 520 (2012).
19. S. Schiller, Appl. Opt. **13,** 2181 (1993).